Earth and Planetary Science Letters 529 (2020) 115875

Contents lists available at ScienceDirect

Earth and Planetary Science Letters

www.elsevier.com/locate/epsl

End-Permian (252 Mya) deforestation, wildfires and flooding—An ancient biotic crisis with lessons for the present

Vivi Vajda [a,*], Stephen McLoughlin [a], Chris Mays [a], Tracy D. Frank [b], Christopher R. Fielding [b], Allen Tevyaw [b], Veiko Lehsten [c], Malcolm Bocking [d], Robert S. Nicoll [e]

[a] Swedish Museum of Natural History, Svante Arrhenius v. 9, SE-104 05, Stockholm, Sweden
[b] Department of Earth and Atmospheric Sciences, University of Nebraska-Lincoln, 126 Bessey Hall, Lincoln, NE 68588-0340, USA
[c] Lund University, Department of Physical Geography and Ecosystem Science, Sölvegatan 12, SE-223 62 Lund, Sweden
[d] Bocking Associates, 8 Tahlee Close, Castle Hill, NSW, Australia
[e] 72 Ellendon Street, Bungendore, NSW 2621, Australia

ARTICLE INFO

Article history:
Received 28 April 2019
Received in revised form 29 September 2019
Accepted 30 September 2019
Available online xxxx
Editor: I. Halevy

Keywords:
Australia
Triassic
extinction
palynology
biodiversity
Amazon

ABSTRACT

Current large-scale deforestation poses a threat to ecosystems globally, and imposes substantial and prolonged changes on the hydrological and carbon cycles. The tropical forests of the Amazon and Indonesia are currently undergoing deforestation with catastrophic ecological consequences but widespread deforestation events have occurred several times in Earth's history and these provide lessons for the future. The end-Permian mass-extinction event (EPE; ~252 Ma) provides a global, deep-time analogue for modern deforestation and diversity loss. We undertook centimeter-resolution palynological, sedimentological, carbon stable-isotope and paleobotanical investigations of strata spanning the end-Permian event at the Frazer Beach and Snapper Point localities, in the Sydney Basin, Australia. We show that the typical Permian temperate, coal-forming, forest communities disappeared abruptly, followed by the accumulation of a 1-m-thick mudstone poor in organic matter that, in effect, represents a 'dead zone' hosting degraded wood fragments, charcoal and fungal spores. This signals a catastrophic scenario of vegetation die-off and extinction in southern high-latitude terrestrial settings. Lake systems, expressed by laterally extensive but generally less than a few-metres-thick laminated siltstones, generally lacking bioturbation, hosting assemblages of algal cysts and freshwater acritarchs, developed soon after the vegetation die-off. The first traces of vascular plant recovery occur ~1.6 m above the extinction horizon. Based on analogies with modern deforestation, we propose that the global fungal and acritarch events of the Permo-Triassic transition resulted directly from inundation of basinal areas following water-table rise as a response to the abrupt disappearance of complex vegetation from the landscape. The $\delta^{13}C_{org}$ values reveal a significant excursion toward low isotopic values, down to −31‰ (a shift of ~4‰), across the end-Permian event. The magnitude of the shift at that time records a combination of changes in the global carbon cycle that were enhanced by the local increase in microbial activity, possibly also involving cyanobacterial proliferation. We envisage that elevated levels of organic and mineral nutrients delivered from inundated dead forests, enhanced weathering and erosion of extra-basinal areas, together with local contributions of volcanic ash, led to eutrophication and increased salinity of basinal lacustrine–lagoonal environments. We propose that the change in acritarch communities recorded globally in nearshore marine settings across the end-Permian event is to a great extent a consequence of the influx of freshwater algae and nutrients from the continents. Although this event coincides with the Siberian trap volcanic activity, we note that felsic–intermediate volcanism was extensively developed along the convergent Panthalassan margin of Pangea at that time and might also have contributed to environmental perturbations at the close of the Permian.

* Corresponding author.
E-mail address: vivi.vajda@nrm.se (V. Vajda).

https://doi.org/10.1016/j.epsl.2019.115875

1. Introduction

Deforestation threatens biodiversity and ecosystem stability at all latitudes and has ensuing effects on the hydrological cycle and climate systems (Aragão et al., 2008). Forests are vital for stabilizing Earth's systems as they buffer the landscape from soil erosion, drought, and flooding, and also provide habitats for animals, understorey plants and microbes (Aragão et al., 2008; Costa and Pires, 2010). Major deforestation events have occurred in tandem with several biotic crises in Earth's history and these may serve as ecological analogues for future environmental change. The terrestrial end-Permian mass-extinction event (EPE) provides a particularly striking global, deep-time analogue for modern deforestation and diversity loss.

Losses of marine animal species during the EPE have been estimated at 80–96% (Stanley, 2016) and some authors argue that the extinction in the oceans was coeval with that on land (Payne and Clapham, 2012), whereas others have presented evidence of extinction on land preceding that in the oceans (Fielding et al., 2019; Mays et al., in press). The EPE in southern high-latitude non-marine successions has long been associated with the disappearance of broad-leafed deciduous forests dominated by glossopterid gymnosperms (Helby, 1970; Foster, 1979; Vajda and McLoughlin, 2007; McLoughlin, 2011; Van de Wetering et al., 2013a, 2013b). Glossopterids supplied nutrition and living space for diverse networks of vertebrates, invertebrates and micro-organisms (Slater et al., 2015) and were the prime contributors of biomass to the vast Permian coal deposits of Gondwana, hence their disappearance had major implications for ecosystem structure.

The detailed biological signal following the EPE is marked by two geographically widespread palynological events, the 'algal/fungal/acritarch event' (a bloom of *Reduviasporonites*, and of acritarchs in marine environments; Eshet et al., 1995; Looy et al., 2001; Kar and Ghosh, 2018; Rampino and Eshet, 2018), and the 'spore-spike event' (Schneebeli-Hermann et al., 2015). The presence of abundant acritarchs in post-extinction continental deposits has contributed to a continuing debate as to whether the EPE interval was marked by eustatic sea-level rise (Thomas et al., 2004). Importantly, high-resolution data from marine settings, e.g. from Finnmark (Norway), Greenland, and Western Australia (Perth Basin) document acritarch blooms of freshwater aspect in marine deposits within the EPE (van Soelen et al., 2018; van Soelen and Kürschner, 2018; Metcalfe et al., 2008; Haig et al., 2015). An understanding of the turnover in terrestrial ecosystems calls for more detailed evaluation of biotic changes in stratigraphically complete continental successions.

The end-Permian event is generally linked to Siberian trap magmatism (Burgess et al., 2017), with recent data revealing anomalously high, probable volcanogenic, mercury (Hg) levels through the EPE (Wang et al., 2019). Although most attention of causal mechanisms for the EPE has focused on emissions from Siberian Trap basaltic volcanism, the effects of the extensive circum-Pangean felsic volcanism (Riel et al., 2018) have been largely overlooked as potential contributors to the environmental crisis.

This study, based on continuous sedimentary successions in the high-paleolatitude foreland Sydney Basin, Australia, documents the highest-resolution palynological signal yet recovered from an end-Permian succession in the Southern Hemisphere. The study aims to identify the end-Permian event horizon and to resolve the ecological changes by drawing analogies with modern deforestation patterns and their consequences.

2. Geological setting, stratigraphy and paleoenvironment

The Sydney Basin was part of a large foreland basin system (the Sydney-Gunnedah-Bowen basin complex) located at 65–75 °S in SE Gondwana at the end of the Permian (Fig. 1a–c) and hosted a large southward-draining axial fluvial system to the west of a continental volcanic arc, the New England Orogen (Fielding et al., 2001; Rosenbaum, 2018). The late Permian was characterized in this region by prolonged regression and, by the end of the period, few marine depositional systems existed within Australia (Shi et al., 2010; Frank et al., 2015). The region had a cool temperate and consistently moist climate during the latest Permian (Lopingian) but general circulation modeling and the chemical index of alteration suggest that the Sydney Basin experienced enhanced seasonality, including higher temperatures and higher precipitation immediately following the EPE, particularly during the summer months warmer and drier summers following the EPE (Fielding et al., 2019). However, the longer term climatic trend shows progressive drying through the Early Triassic (Metcalfe et al., 2015; Mays et al., in press).

This is consistent with the occurrence of numerous false (intraseasonal) rings in Early Triassic wood from this basin (Baker, 1931), together with an increase up-section of sedimentary features indicative of seasonal drought, such as desiccation structures, ferruginous concretions, and microspherulitic siderite in Narrabeen Group paleosols (Retallack, 1999). Paleoclimatic interpretations across the EPE in the Sydney Basin based on paleosol geochemistry (Retallack, 1999) have suggested mean annual precipitation of 1000–1300 mm during deposition of both the latest Permian coal-bearing succession and the immediately succeeding post-EPE charcoal-rich strata, but with reduction to 800–1200 mm per annum during deposition of the upper part of the Dooralong Shale (~1–11 m above the coal; Fig. 2a, b).

Volcanoes along the New England Orogen (Fig. 1c) supplied numerous ash beds to the adjacent foreland basin from which zircon CA-ID-TIMS radiogenic U-Pb age estimates have enabled recalibration of the eastern Australian Permian–Triassic palynostratigraphic zones (Metcalfe et al., 2015; Laurie et al., 2016). These methods have now tightly constrained the position and age of the terrestrial EPE in the Sydney Basin succession to between 252.60 ± 0.04 Ma and 252.31 ± 0.07 Ma (Fielding et al., 2019).

Upper Permian successions across the Sydney Basin comprise multiple cycles of coastal plain fluvial channel sands, floodbasin mudstones, coals and tuffs that are assigned to several units within the upper Newcastle Coal Measures (Fig. 2a, b). The uppermost unit of the coal measures, informally named the Vales Point coal, represents peat accumulation immediately preceding the EPE (Fig. 2a, b). The conformably overlying Dooralong Shale and Munmorah Conglomerate (Narrabeen Group) extend into the lowermost Triassic (Fig. 2a, b).

The Global Stratotype Section and Point (GSSP) of the Permian-Triassic Boundary (separating the Changhsingian and Induan stages) was ratified in 2001 (Yin et al., 2001), whereby the boundary was defined at the first occurrence of the conodont *Hindeodus parvus*, i.e., at the base of Bed 27c of the Meishan section D, in Changxing County, Zhejiang Province, South China. As this conodont index taxon represents a component of the recovery fauna that evolved following the extinction, a significant lag time (of at least tens of thousands of years) will always exist between the initial pulse of the end-Permian extinction event (dated as 251.941 ± 0.037 Ma: Bed 25 at Meishan) and the subsequent appearance of *H. parvus* defining the Permian–Triassic boundary in the marine successions (dated as 251.902 ± 0.024 Ma: Bed 27c at Meishan; Burgess et al., 2014). No internationally recognized reference section exists for the Permian–Triassic boundary in non-marine settings, although several successions in the Sydney Basin have the potential to serve as excellent continental stratotype sections. The major challenge posed for determining global correspondence of events around the PTB is the correlation between marine and non-marine realms and their biotas. Therefore, we consistently refer to the terrestrial end-

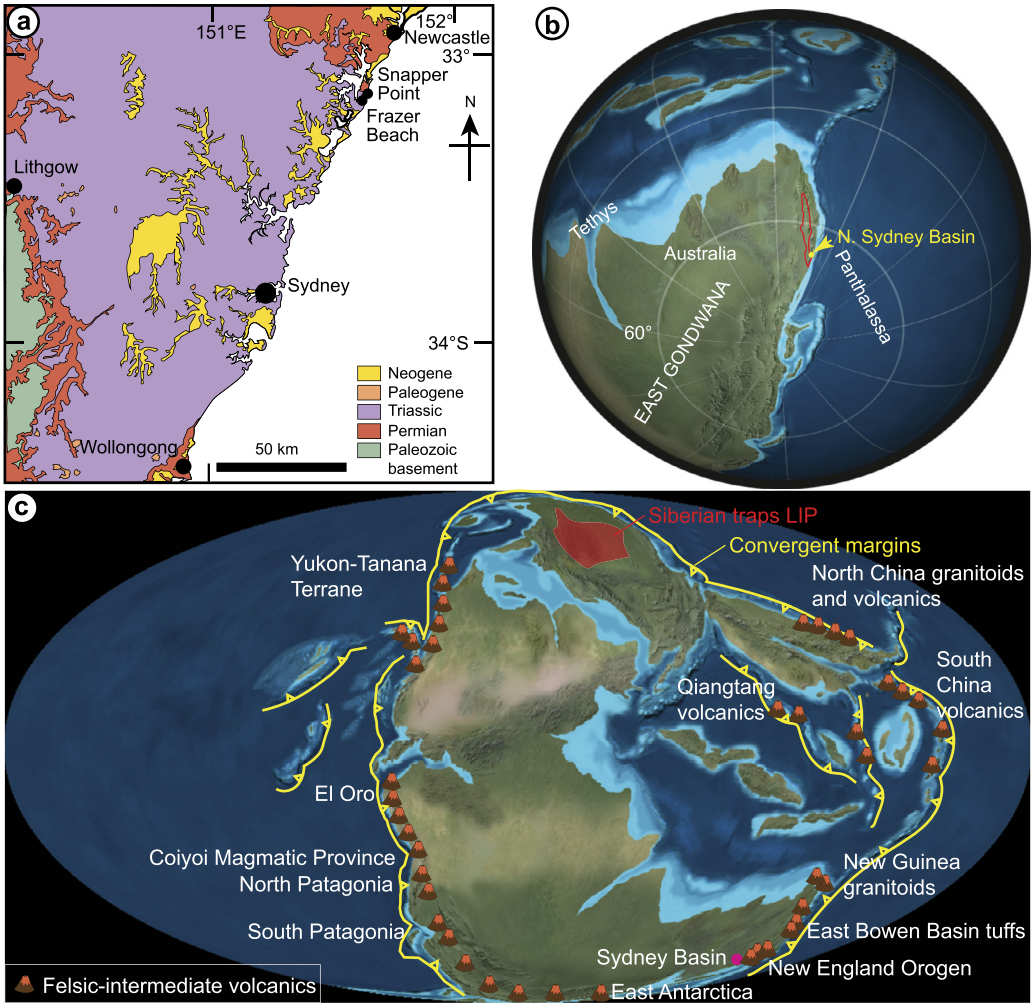

Fig. 1. Stratigraphic and palaeogeographic setting of the successions spanning the end-Permian event in the Sydney Basin, Australia. **a)** Map of the Sydney Basin showing the distribution of Permian and Triassic strata. **b)** Late Permian paleogeographical map of eastern Gondwana with the study area marked immediately to the west of a continental volcanic arc flanking the southeastern margin of Gondwana. At the end of the Permian, the Sydney Basin formed the southern part of a >2000-km-long, meridional, asymmetrical foreland basin, the Bowen-Gunnedah-Sydney basin complex (outlined in red). It is likely that this foreland basin complex of ~240 000 km^2 was drained by a common fluvial system that issued southward to enter the sea east of the current limits of the Sydney Basin. **c)** Global paleogeographic map for the Permian-Triassic transition showing the location of the Siberian Traps Large Igneous Province, the distribution of subduction zones (yellow lines), and felsic magmatism (volcano symbols) forming the Pangean 'ring of fire' (base maps adapted from Blakey, 2005, with additional information from Zhang et al., 2013; Amiruddin, 2014; Ye et al., 2014; Liao et al., 2016; Riel et al., 2018; Spalletti and Limarino, 2017; Jessop et al., 2019). (For interpretation of the colors in the figure(s), the reader is referred to the web version of this article.)

Permian event herein (not to the Permian–Triassic boundary *sensu stricto*) and use the EPE as the reference datum point in the studied sections.

3. Material and methods

Cliff sections at Snapper Point (33°11′13.35″S, 151°37′42.00″E) and Frazer Beach (33°11′37.21″S, 151°37′22.34″E), Munmorah State Conservation Area, New South Wales, Australia, were logged and sampled in detail for the distribution of sedimentary facies, geochemistry, palynomorphs and plant macrofossils (Figs. 1–7).

3.1. Palynology and paleobotany

Forty-nine palynological samples were collected through a 13.1-m-thick succession at Frazer Beach and 24 samples through a 2-m-thick section at Snapper Point, providing a composite profile through the Vales Point coal seam and Dooralong Shale, and spanning the EPE (Figs. 1–3; Supplementary online Fig. S1). Samples of ~15 grams were processed according to standard procedures at Global Geolab Limited, Canada, incorporating treatment with hydrochloric (HCl) and hydrofluoric (HF) acids in order to remove carbonates and silicates, and subsequent sieving of residues with a 5 µm nylon mesh. The organic residue was mounted in epoxy resin on microscopy slides, and the organic matter was classified according to the scheme developed by Batten (1996). The following palynofacies categories were distinguished: charcoal, wood remains, plant cuticles, bisaccate non-taeniate pollen, bisaccate taeniate pollen, plant spores, algae, acritarchs and fungi. Biostratigraphic analysis involved scanning two microscopy slides per sample for key taxa. Quantitative evaluation involved palynofacies analysis by scoring the relative abundance of organic particles based on 300 counts per slide; results shown in Supplementary Material (Table S1). Plant macrofossils were prepared from bedding planes by dégagement and photographed with low-angle light from the upper left. The slides and residues and most macrofossils are stored in the collections of the Swedish Museum of Natural History, Stockholm, Sweden (prefixed NRMS). One fossil leaf is held in the W.B. Clarke Geoscience Centre, Londonderry, New South Wales, Australia (prefixed MMF).

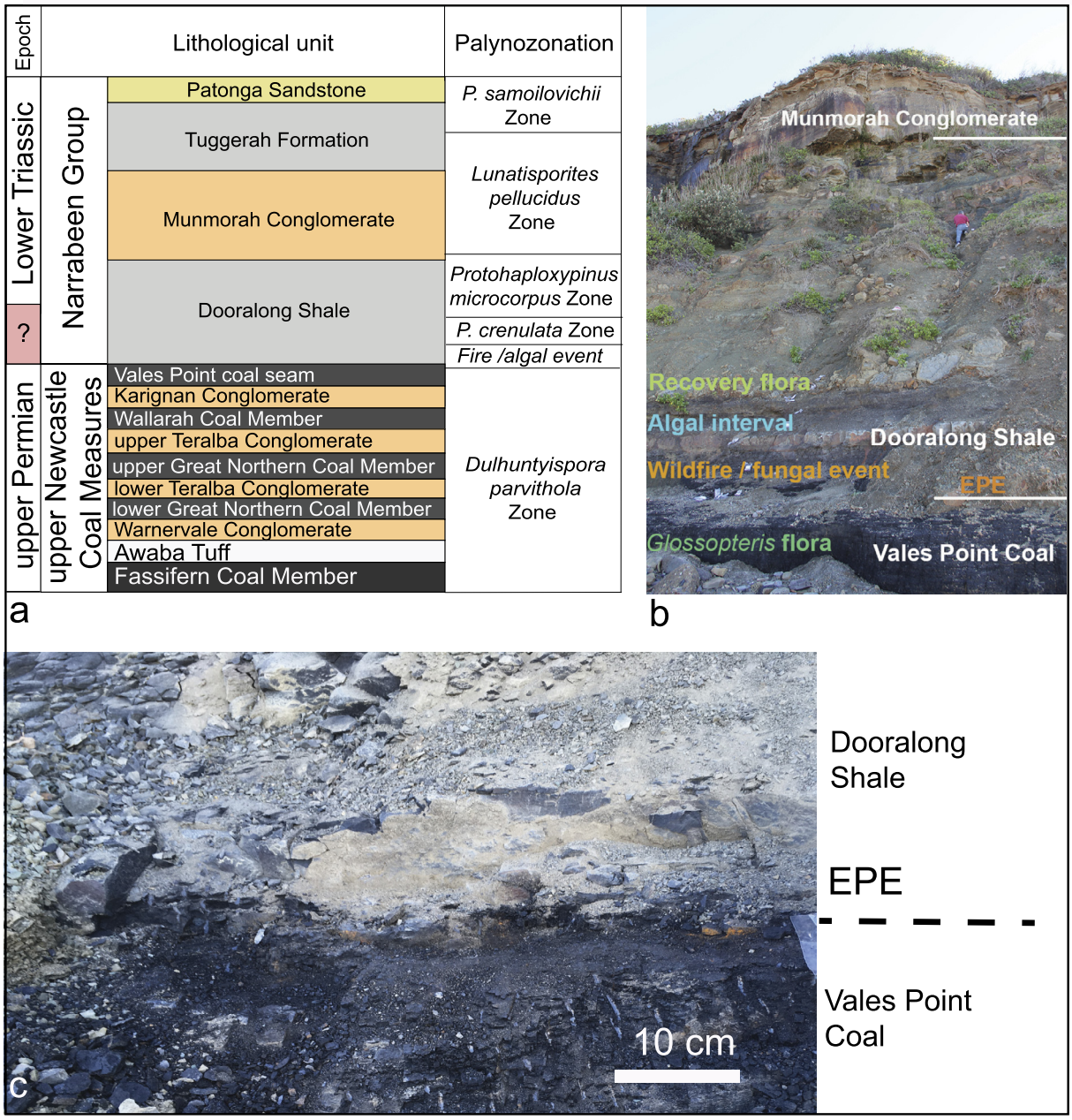

Fig. 2. a) Chronostratigraphic, lithostratigraphic, and palynostratigraphic scheme for the Permian–Triassic transition of the northern Sydney Basin. **b)** Photograph of the Frazer Beach section, ~16 m high. Note human scale Stephen McLoughlin, 176 cm. **c)** Details of the transition from coal to mudstone marking the EPE at Frazer Beach.

3.2. Geochemistry

C-N concentrations and isotopic compositions of bulk organic matter were analyzed for 34 samples through the 13.1-m-thick succession spanning the EPE at Frazer Beach and for 24 samples through the 2-m-thick section at Snapper Point (Tables S2, S3). In preparation for analysis, splits of samples used for the palynological study were powdered, reacted for 24 h with 1N HCl at room temperature to remove inorganic carbon, and rinsed three times in ultra-pure water. In each case, the supernatant was separated by centrifugation and discarded. Samples were then dried in an oven at 40 °C and re-crushed using an agate mortar and pestle. Total organic carbon (TOC), total nitrogen (TN), and carbon and nitrogen isotope compositions were determined by high temperature combustion using a Costech 4010 Element Analyzer connected to a Thermo Finnigan MAT 253 stable-isotope gas-ratio mass spectrometer in the W.M. Keck Paleoenvironmental and Environmental Stable Isotope Laboratory at the University of Kansas. Carbon isotope compositions of bulk organic matter fractions are reported in per mille (‰) relative to Vienna PeeDee Belemnite (VPDB), whereas nitrogen isotope compositions are reported in per mille (‰) relative to Air. Analyses of working standards (DORM, ATP) were reproducible to better than ±0.13‰ (1σ SD) for δ^{13}C and ±0.39 (1σ SD) for δ^{15}N.

4. Results and interpretation

4.1. The vegetation signal

The palynological results reveal a succession of abrupt events at the close of the Permian. Rich and well-preserved miospore assemblages dominated by taeniate (striate) bisaccate pollen grains (Figs. 3–4) assigned to the *Dulhuntyispora parvithola* Zone of latest Permian age occur below and within the Vales Point coal

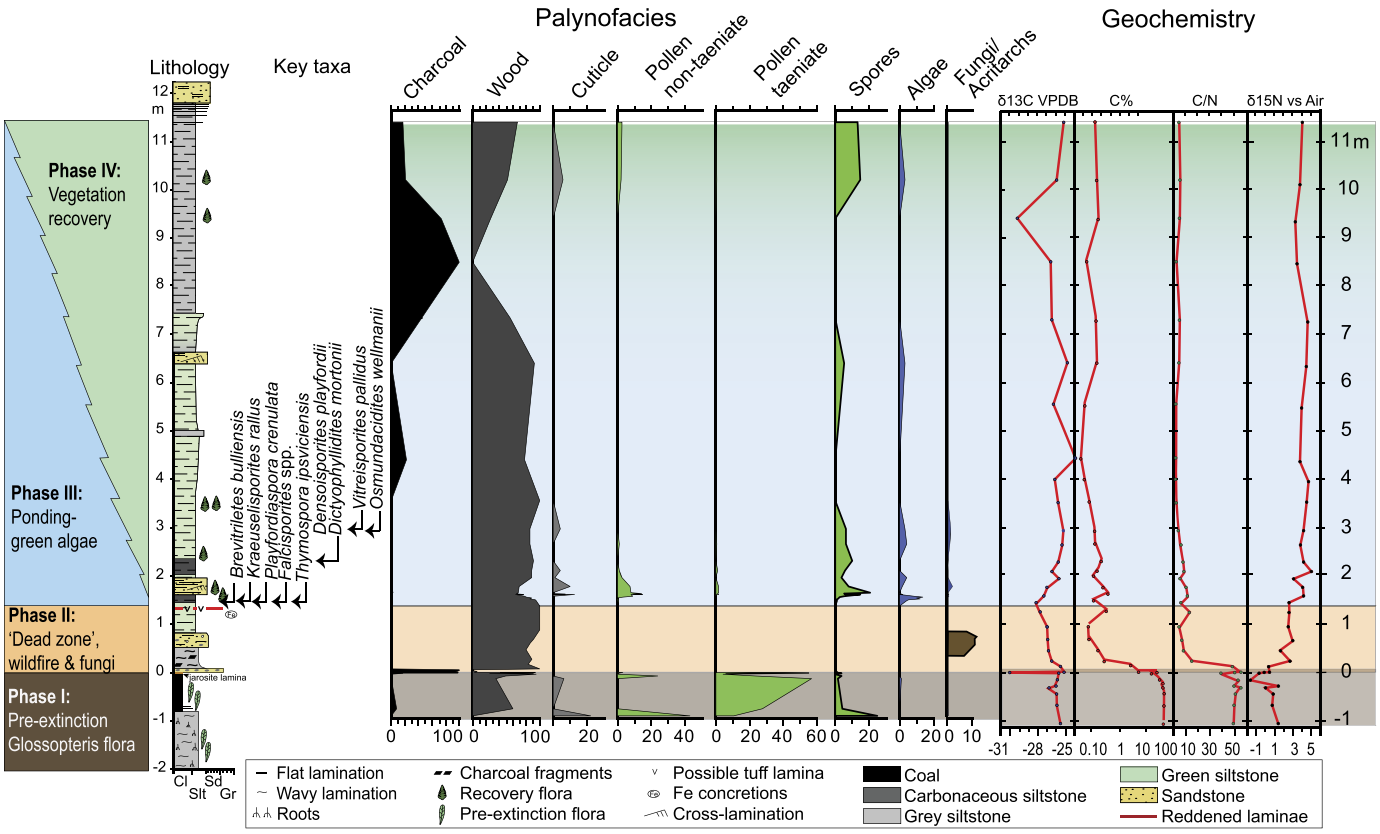

Fig. 3. Graphical log of the Frazer Beach section. Stratigraphy is tied to the chronostratigraphic scale using CA-ID-TIMS U-Pb ages from Fielding et al. (2019). Selected palynofacies/miospore groups recovered from outcrop samples reveal a major turnover in the floras at the top of the Vales Point coal inferred to represent the EPE. First appearance datums of selected palynomorph taxa provide the basis for recognizing the local palynozones.

seam (both within the coal and in shale partings), denoting complex glossopterid-dominated communities with high spore-pollen productivity. The Vales Point coal is dominated by compressed glossopterid wood and leaves (occurring as vitrinite), and the underlying siltstones (paleosol) contain abundant glossopterid roots (*Vertebraria*: Fig. 5f) denoting a forested mire ecosystem. Diverse palyno-assemblages persist seemingly unaltered up to the top of the Vales Point coal but overlying strata are devoid of glossopterid pollen and leaves. The contact between the coal and the overlying carbonaceous mudstone is marked by a layer rich in jarosite ($KFe_3^{3+}(OH)_6(SO_4)_2$) at both sites. A sharp decrease in organic matter content occurs at this level, and assemblages from the succeeding 20 cm are strongly dominated by woody debris—a significant portion of which is charcoalified (Fig. 3). This major shift is evidence of an abrupt die-off of the glossopterid mire communities and is mirrored in the sedimentological record at the studied sites by the abrupt change from coal to a muddy polymict micro-breccia (containing quartz grains, amorphous siliceous possible pumice clasts, and sub-angular clay-pellets and coal fragments) extending 0–20 cm above the coal. This grades upward into a grey siltstone (20–55 cm above the coal) in which the palynological assemblages are characterized by translucent phytodebris, algal thalli, fungal spores and abundant phytoclasts degraded through bacterial activity, and this interval is herein designated 'the dead-zone'. (Fig. 2c). An overlying crevasse-splay sand lacks significant palynomorphs apart from wood.

A succession of assemblages rich in fresh- or brackish-water algae initiates in siltstones at 140 cm above the coal, above a thin iron-stained tuffaceous layer (Figs. 3, 6a–n). These assemblages are dominated by green algae, including the zygnematalean microalga *Circulisporites parvus* (Fig. 6h, i, m, n), and leiospheres, which are thin-walled, smooth to weakly ornamented, spherical cysts of unknown algal affinity (Lindgren, 1981; Fig. 6f, g, k, l), with subordinate *Quadrisporites horridus* (Fig. 6j), attributed to the freshwater green algae Scenedesmaceae; Batten, 1996), and sparse examples of the spinose acritarch *Micrhystridium* sp.

Land vegetation (vascular plant) recovery is marked by the appearance of new spore/pollen taxa in a laminated sandy siltstone ~160 cm above the Vales Point coal at Frazer Beach (Figs. 3, 5a–e, h–k). This palynoassemblage is dominated by fern and lycophyte spores, spore clusters, and bisaccate non-taeniate pollen (Fig. 4a–n) of typical Triassic seed-ferns and conifers (Fig. 5). These beds also yield a macroflora (Fig. 5a–d, h–k) comprising leaves and stems of a peltaspermalean seed-fern (*Lepidopteris callipteroides*: Fig. 5a, b, h, i), voltzialean conifer (*Voltziopsis* spp.: Fig. 5j), a ginkgoalean (*Ginkgophytopsis* sp.: Fig. 5k), isoetaleans (*Isoetites* sp.), equisetaleans (*Neocalamites* sp.), together with various dispersed plant cuticles (Fig. 5c–e). These are among the earliest post-EPE plants yet documented globally, providing direct insights into the structure of the immediate recovery vegetation.

4.2. Geochemistry

The total organic carbon values (TOC) show a major change through the sections, with average values of between 5 and 10% C in the uppermost Permian siltstones below the Vales Point coal (Fig. 3). The TOC within the coal averages ~56% at Frazer Beach (range 23–71%), and ~40% at Snapper Point (range 7–69%) where a larger variance is evident owing to more silty laminae (see Supplementary Material, Tables S2, S3). The TOC drops to an average of 6% in the charcoal-dominated interval and drops sharply above that to values consistently below 1% at both sites (range 0.53–0.05% at Frazer Beach, 0.22–0.62% at Snapper Point).

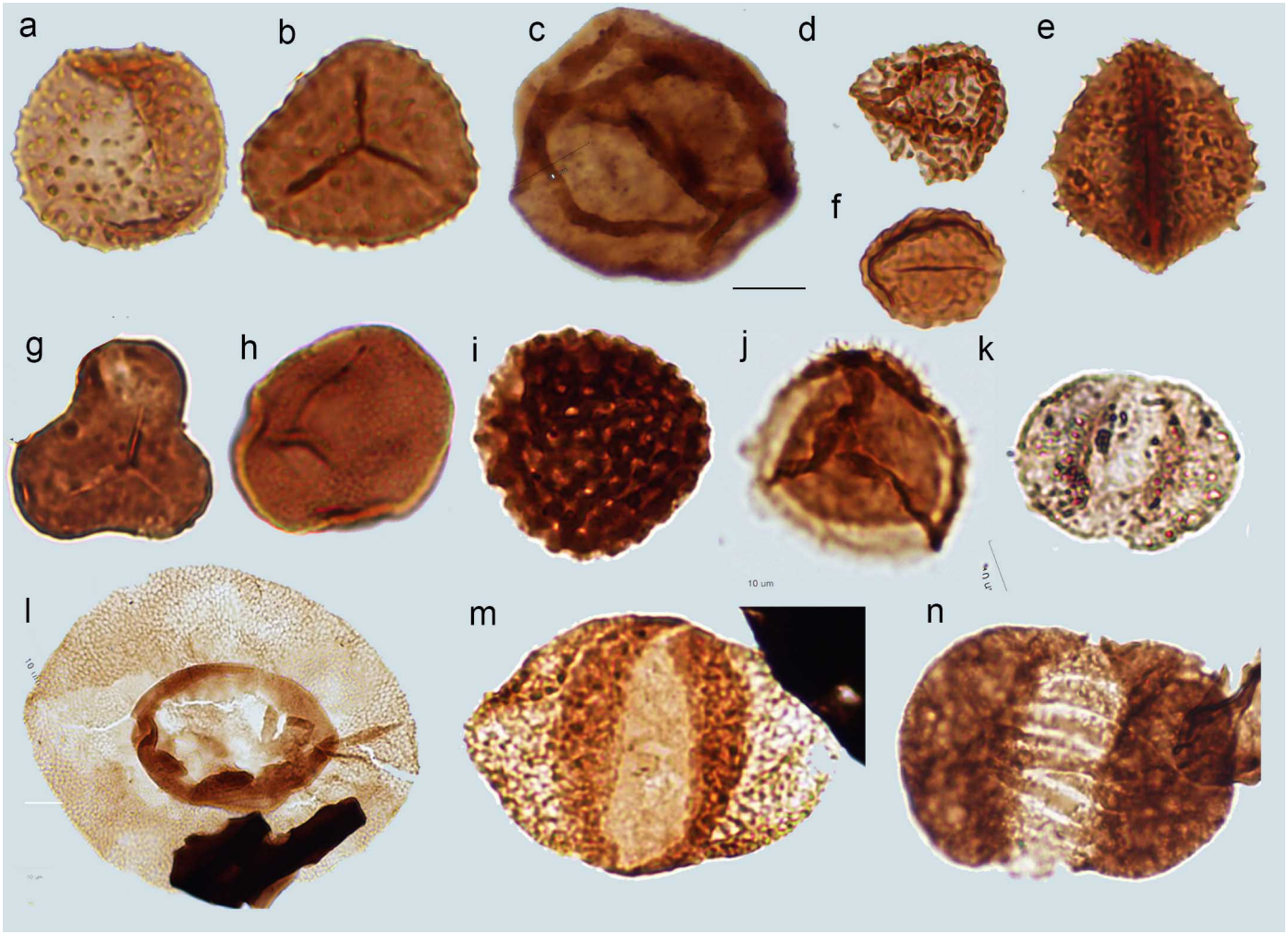

Fig. 4. Light-micrographs of selected spores and pollen identified in the post-extinction mudstone at the Frazer Beach section. **a)** *Brevitriletes bulliensis*; **b)** *B. bulliensis*; **c)** *Osmundacidites wellmanii*; **d)** *Retitriletes rugulatus* **e)** *Brevitriletes* sp.; **f)** *Thymospora ipsviciensis*; **g)** *Concavissimisporites* sp.; **h)** *Cyclogranisporites* sp.; **i)** *Foveosporites moretonensis*; **j)** *Kraeuselisporites rallus*; **k)** *Vitreisporites pallidus*; **l)** *Playfordiaspora crenulata*; **m)** *Falcisporites* sp.; **n)** *Protohaploxypinus jacobii*.

The $\delta^{13}C_{org}$ values through the Frazer Beach section show a significant range, from -31.1‰ to -24.5‰ (average -25.9‰; Fig. 3; Table S2). The lowest values occur in the sample from 4 cm above the Vales Point coal and in the sample at 146 cm, in which the organic matter is dominated by algae. Likewise, the most ^{13}C -depleted values (-27.4‰) occur within the topmost sample of the Snapper Point section associated with algal-rich assemblages (Table S3). Algae discriminate against the heavier ^{13}C isotope, preferring the lighter ^{12}C isotope. Consequently, these low values are consistent with high algal productivity (Torres et al., 2012) identified at the level of the initial algal spike. This relationship is decoupled higher in the section. This possibly reflects ^{13}C-enrichment of dissolved inorganic carbon (DIC) in hyper-eutrophic lakes resulting from very high primary productivity (Torres et al., 2012).

The C/N ratios range between 1.8 and 57.7 at Frazer Beach and between 9.1 and 57.5 at Snapper Point (Fig. 3; Tables S2, S3). The values at the two sites are very consistent, with C/N ratios decreasing significantly at ~25–40 cm above the coal and with the lowest values at the very top of the Frazer Beach section). The high C/N ratios within the coal and the charcoal-dominated samples are consistent with the prominence of lignin-rich terrestrial plants, whereas the low C/N ratios in the overlying charcoal-rich interval are consistent with the lacustrine algal source of the organic matter (Torres et al., 2012).

The $\delta^{15}N$ values range from −1.7 to 5.0‰ through the succession (Fig. 3, Tables S2, S3), with the higher values registered consistently above the EPE and the lowest levels occurring in the uppermost levels of the coal, and in the base of the charcoal-dominated interval. $\delta^{15}N$ values are generally difficult to interpret but the systematic shifts towards higher values in the intervals dominated by algae, possibly signals high nutrient availability (eutrophication) in the palaeo-lake system.

4.3. Ecological consequences of deforestation

The consequences of deforestation on the scale of entire sedimentary basins are not known from modern systems, but examples of extensive deforestation from early human settlements in New Zealand and Australia (Woodward et al., 2014), and the ecological impact of modern deforestation in such diverse settings as Australian woodlands (Ruprecht and Schofield, 1991a, 1991b), Tibetan alpine forests (Cui et al., 2007), the Amazon Basin tropical forests (Gentry and Lopez-Parodi, 1980; Marengo and Espinoza, 2015), southeast Asian raised mire systems (Wells et al., 2016), and Siberian temperate forests (Burenina et al., 2014) are well known. The ecological impacts of modern deforestation in these diverse vegetation types typically include an abrupt decline in biodiversity, increased soil erosion, and nutrient loading of watercourses (Ruprecht and Schofield, 1991a, 1991b; Cui et al., 2007).

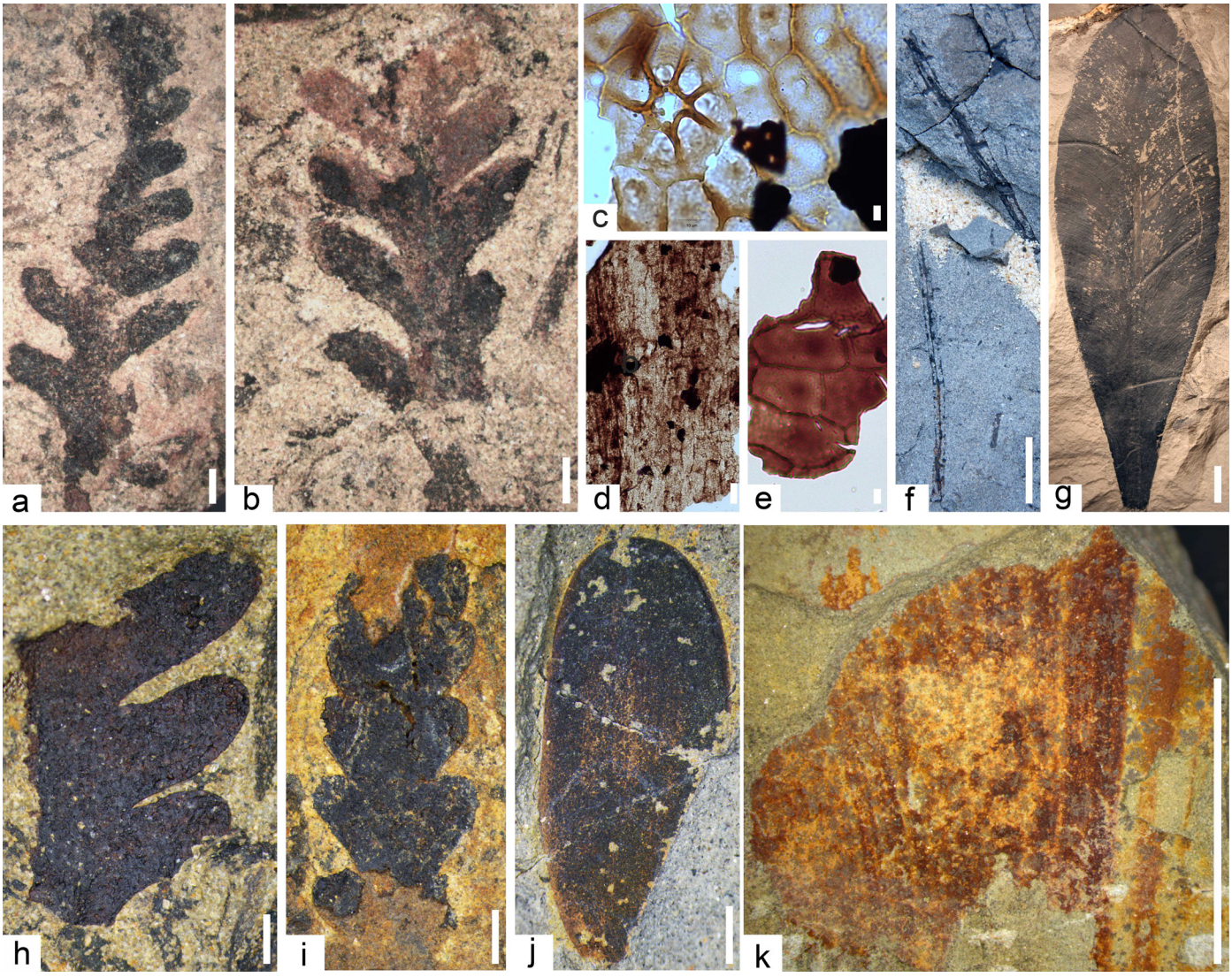

Fig. 5. Plant macrofossils and dispersed cuticle fragments from the Permian–Triassic transition in the northern Sydney Basin. **a**, **b**, **h**, **i**) *Lepidopteris callipteroides* (peltasperm seed-fern) pinna fragments showing the variation in pinnule morphology; 1.6–1.8 m above top of Vales Point coal seam at Frazer Beach; NRMS08794, NRMS08793, NRMS08792-01, NRMS0872-02, respectively. **c**) *Lepidopteris callipteroides* dispersed cuticle fragment showing stoma with seven subsidiary cells and papillae overhanging the aperture; NRMS. **d**) Dispersed cuticle of possible coniferous affinity with elongate rectangular cells; 1.59 m above top of Vales Point coal seam at Frazer Beach; NRMS. **e**) Dispersed cuticle of possible corystosperm (Umkomasiaceae) affinity having short, polygonal, uni-papillate cells with slightly buttressed sinuous anticlinal cell walls; 1.76 m above top of Vales Point coal seam at Frazer Beach; NRMS. **f**) *Vertebraria australis*, segmented glossopterid roots preserved in siltstone 2 m below the top of the Vales Point coal seam at Frazer Beach. **g**) *Glossopteris browniana* leaf typical of uppermost Permian strata in the northern Sydney Basin; MMF2884. **j**) *Voltziopsis africana* conifer leaf from 1.6–1.8 m above top of Vales Point coal seam at Frazer Beach; NRMS089791. **k**)? *Ginkgophytopsis* sp. leaf fragment with divergent dichotomous venation from 1.6–1.8 m above top of Vales Point coal seam at Frazer Beach; NRMS089790. Scale bars = 1 mm for **a, b, g–i**, 10 μm for **c**, 10 mm for **e, f, j**.

Importantly, the loss of forests dramatically disrupts the hydrological cycle resulting in regional reduction of precipitation (Aragão et al., 2008; Costa and Pires, 2010; Haas et al., 2019). Roughly, two-thirds of the water precipitated on modern forests is recycled to the atmosphere via evapotranspiration and there are major differences in evapotranspiration rates between bare soil and areas covered by various vegetation types depending on foliar surface area and the developmental stage of the plants (Stan et al., 2014). Despite decreased rainfall in some areas, water-tables become markedly elevated following deforestation with rises of up to 25 m documented in some valleys, turning lowland areas into swamps or salt marshes (Ruprecht and Schofield, 1991a, 1991b). Flooding of the landscape following deforestation is caused by a combination of reduced canopy interception of precipitation, lesser groundwater uptake by plant roots, decreased evapotranspiration and, on a seasonal basis, overbank flooding from increased peak flow rates in watercourses (Díaz et al., 2007).

Upper Permian coals and permineralized peats of the Sydney-Gunnedah-Bowen basin system are overwhelmingly dominated by the remains of glossopterid gymnosperms (Diessel and Smyth, 1995; McLoughlin et al., 2019) suggesting these plants were the main constituents of the immediate peat-forming ecosystems. Seatearths beneath the coal seams are typically rich in *Vertebraria* (glossopterid) roots with internal air chambers, interpreted to be an adaptation for growth in waterlogged substrates. These features attest to the growth of glossopterids within the mire system proper. Permineralized and coalified stumps and logs preserved within the Upper Permian coals are up to 1 m in diameter (McLoughlin, 1993), indicating that these trees probably reached 30 m tall based on the scaling relationships of modern gymnosperm stems (Niklas, 1994; Gulbranson et al., 2012).

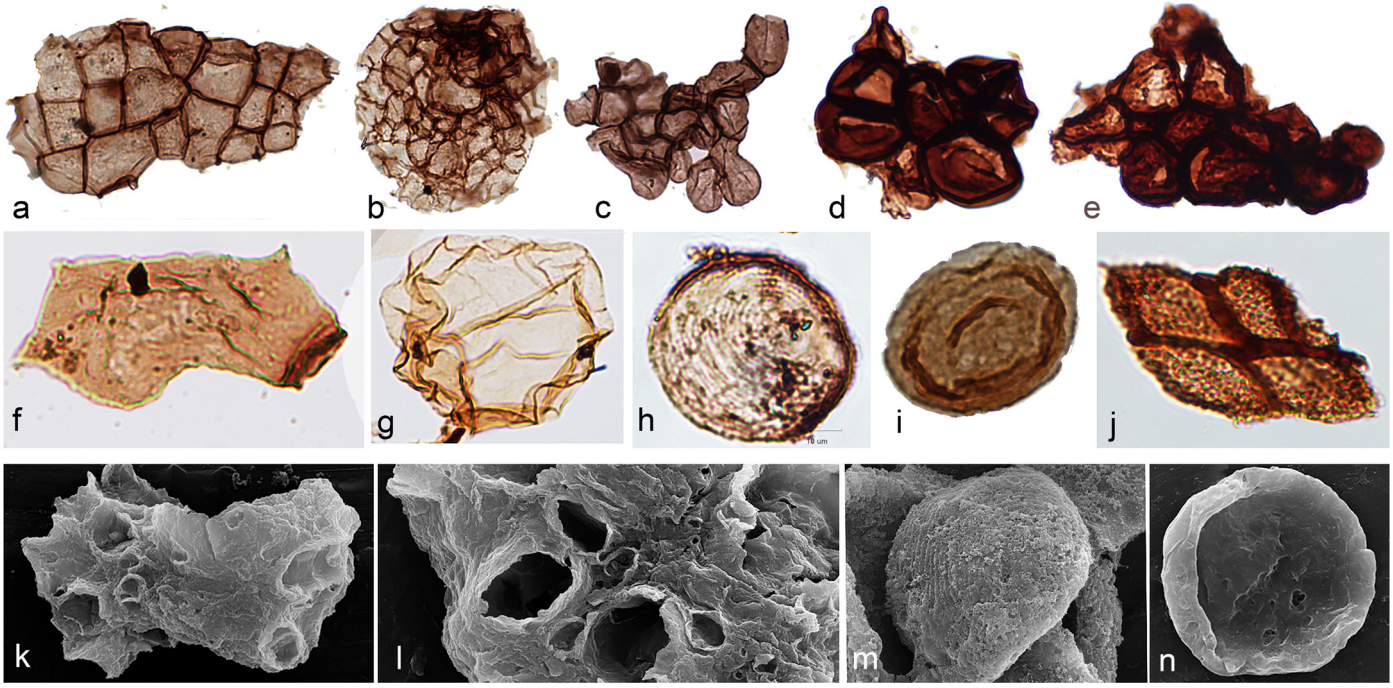

Fig. 6. Light micrographs of fungi, algal thalli and algal cysts. **a–e)** Algal thalli and fungal colonies; **a–b**) Algal thalli; **c)** Fungal colonies; **d–e)** Enlargement of fungal colonies; **f)** *Reduviasporonites* sp.; **g)** *Leiosphaeridia* sp.; **h–i**) *Circulisporites parvus*; **j)** *Quadrisporites horridus*; **k–n**) Scanning electron micrographs of selected algae; **k)** *Leiosphaeridia* sp. with pockmarks from pyrite; **l)** Enlargement of pockmarks; **m–n)** *Circulisporites parvus*; **m)** proximal side, **n)** distal side.

Glossopterids are interpreted to have been tall, relatively conical, and moderately well-spaced in order to optimize interception of low-angle light at high latitudes. They were deciduous trees with reticulate-veined, spathulate leaves, typically around 10–15 cm long and 2–3 cm wide (Fig. 5g). Boreal deciduous birch (*Betula*) or larch (*Larix*) forests of swampy environments are considered by some authors as modern analogues of Permian glossopterid forests (Izart et al., 2015). Although no consensus has been reached on the hydrology of the high-latitude late Permian peats, they are commonly envisaged to have developed as laterally extensive, low-gradient, forested, raised (ombrogenous) mires supported by high precipitation rates and low evapotranspiration (Clymo, 1987; Slater et al., 2015). Ground-cover elements of the Gondwanan forests, and open plant communities along watercourses and lake margins comprised mainly herbaceous ferns, sphenopsids, and lycophytes (Holmes, 1995; McLoughlin et al., 2019).

Processes following modern deforestation provide a template for the environmental changes related to the extinction of glossopterid forests at the EPE. We identified four main phases (I–IV) in this biotic turnover (Figs. 3, 7) that are outlined below. The duration of each phase is a rough estimate based on accumulation rates through the upper Permian and Triassic succession in the Sydney Basin. Based on the radiometrically calibrated succession in the central Sydney Basin (Metcalfe et al., 2015; Fielding et al., 2019), we calculated accumulation rates at ~13,000 yrs/m for the Upper Permian continental, delta plain deposits and ~7900 yrs/m for the post-extinction successions of the Narrabeen Group. We also compared these values to calculations of sedimentation rates of continental Cretaceous–Paleogene boundary strata of the Fort Union Formation in North Dakota (Hicks et al., 2002; Noorbergen et al., 2018) because the K–Pg boundary provides the best-dated timeline for any mass extinction event (Schulte et al., 2010; Renne et al., 2018). Moreover, the Paleogene terrestrial sediments accumulated following denudation of forests following the Chicxulub impact event, providing a similar environmental signal. The calculated accumulation rates from the Sydney Basin are fairly consistent with those from the Western Interior Williston Basin (K–Pg boundary) for the pre-extinction depositional systems where an accumulation rate of ~10,465 yrs/m is evident for the Maastrichtian Hell Creek Formation (Hicks et al., 2002). A lower accumulation rate of ~13,275 yrs/m was calculated for the lower Palaeocene Tullock Member of the Fort Union Formation (Noorbergen et al., 2018)—a rate that is also substantially lower than that calculated for the post-extinction succession in the Sydney foreland basin system.

4.4. Stages of extinction and recovery

4.4.1. Phase I. Extinction of the Permian flora

Little change is evident in the Permian palyno- or macrofloras preceding the EPE either in the studied sections or in other parts of the Sydney Basin (Fielding et al., 2019). Low-diversity, glossopterid-dominated mire communities incorporating a modest range of understorey ferns, sphenophytes and lycophytes appear to have been the norm through the entire late Permian. Sedimentary successions record a gradual shift from coastal/deltaic to fully alluvial (fluvio-lacustrine) conditions in the basin through the Lopingian (Fielding et al., 2019), but there is no dramatic signal of change in depositional style leading up to the EPE. Extinction of the glossopterid forested mire ecosystems appears to have been abrupt and is marked in the sedimentary record by the termination of peat accumulation in the Snapper Point and Frazer Beach sections, and in other parts of southern Gondwana.

4.4.2. Phase II. 'Dead zone', wildfire, fungal, and bacterial activity (0–140 cm above the coal)

This interval is represented at Frazer Beach and Snapper Point by a basal 'microbreccia' bed (stratigraphic height: 0–20 cm) comprising angular intraclasts of coal and siltstone intermixed with possible pumice and sub-angular quartz grains set in a muddy matrix. This is overlain by a mudstone-dominated interval incorporating a single splay-sandstone bed. The basal microbreccia records a brief interval of erosional reworking of the peat surface. A shallow lacustrine setting is inferred for the mudstone-dominated in-

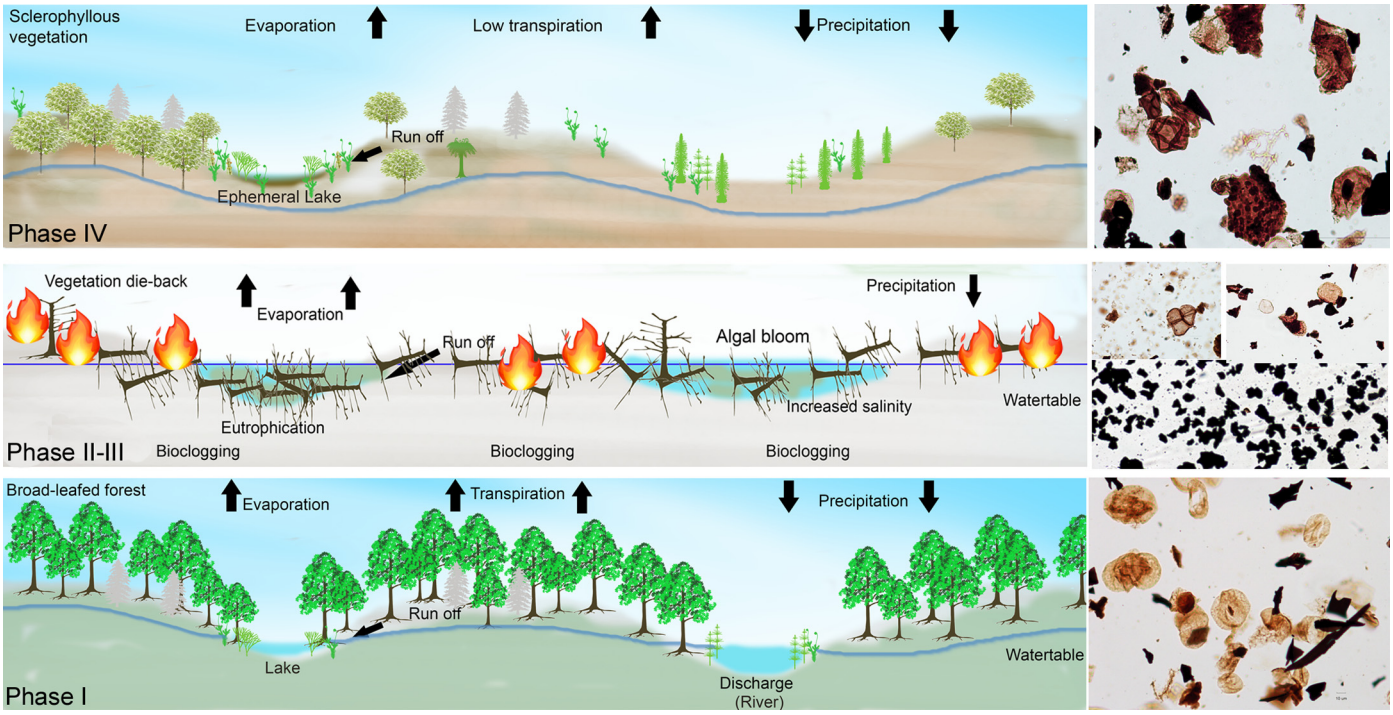

Fig. 7. Reconstruction of ecological successions, before and after the end-Permian event. Light-micrographs (right) show representative palynofacies for each phase. **Phase I:** Thriving typical late Permian mires dominated by glossopterids. **Phase: II–III**: Devastated landscape, degrading organic matter, wildfires, enhanced microbial activity, ponding with algal blooms. **Phase IV:** Open vegetation dominated by opportunistic (ruderal) herbaceous pteridophytes and small-leafed sclerophyllous gymnosperms, growing mainly along water courses in otherwise dry landscape.

terval. The palynofacies in this interval lacks pollen and land plant spores, and incorporates only wood fragments, charcoal, algal thalli and fungal spores. This essentially represents a 'dead zone' in the palaeobiota and is apparently equivalent to the fungal event in the global EPE record outlined by Rampino and Eshet (2018). The immediate effects of the abrupt vegetation die-off, thus, included a large exposed biomass of dead woody plant matter and peat surfaces prone to wildfires. Cessation of water-uptake by roots and evapotranspiration by the canopy would have resulted in the steady elevation of groundwater levels. Although enhanced volcanism and crustal loading characterized the New England Orogen through much of the late Permian, we do not detect a tectonic signal specific to the brief post-EPE lacustrine interval investigated in this study. The pulses of crustal loading occurred over time scales that are one to two orders of magnitude longer than the ponding episode identified following the EPE and are unlikely to represent a causal mechanism for the development of short-lived lacustrine conditions in diverse foreland and epicratonic basins spread across a broad region of southern Gondwana.

Enhanced run-off and erosion likely affected upland areas shortly after regional deforestation, and accumulations of large woody debris, together with continuing compaction and subsidence of the peat surface on floodplains and in valleys would have changed sediment dispersal patterns on a local basis and facilitated ponding in the landscape. The extensive dead biomass in floodbasin settings would have nurtured enhanced fungal, saprotrophic bacterial and cyanobacterial activity. Bacterial reduction of iron in these stagnant lakes contributed to pyrite accumulation—later oxidized to jarosite and iron-oxide staining above the Vales Point coal. This microbial activity, possibly in combination with changes to the global carbon cycle, likely accounts for the significantly lower $\delta^{13}C_{org}$ values at the base of this interval (Fig. 3). An equivalent thin unit of similar sedimentological aspect has been described informally as the 'marker mudstone' in the adjacent Galilee Basin (Wheeler et al., in press). Local erosional pulses contributed sporadic gravelly to sandy channel deposits within this otherwise mudstone-dominated interval. Similar patterns of sedimentation are recorded elsewhere across southern Gondwana in the form of claystone breccias/conglomerates in the Transantarctic Mountains and Karoo Basin (Retallack, 2005), and charcoal enrichment in both continental (Brookfield et al., 2018) and shallow marine (Thomas et al., 2004; Tewari et al., 2015) settings immediately following the EPE.

Estimated duration: 10,000–20,000 yrs.

4.4.3. Phase III. Ponding of the landscape—algae-dominated eutrophic lake systems (140–400 cm above the coal)

The absence of tall woody vegetation, enhanced run-off from upland settings, and decreased soil porosity caused by grain sorting and bioclogging (Fig. 8) from soil microbes, together with rising groundwaters, led to the development of initially detritus-rich lake systems. The combination of intensified seasonality following the EPE and increased nutrient loading, especially by iron and phosphorus from local volcanic sources in the New England Orogen, generated strong fluctuations in water levels, salinity, nutrient status, and pH in floodbasin wetlands.

Seasonal, eutrophic, brackish lake systems developed widely on floodplains, reflected by the accumulation of laterally extensive thin lacustrine facies initiating at 140 cm, and extending to 420 cm, above the coal in the Frazer Beach section. Development of shallow lacustrine facies at this time was a basin-wide phenomenon, as the uppermost Permian coal seam throughout the Sydney and adjacent basins is typically overlain by laminated grey siltstones lacking significant bioturbation. This basal interval is absent at many sites across the basin owing to removal by downcutting of Triassic fluvial systems. In the studied succession, the various brackish–freshwater algal taxa flourished under the consumer-poor, eutrophic lacustrine conditions, as evidenced by successive algae-dominated palyno-assemblages in laminated mudstones 140–400 cm above the level of the EPE. Equivalent beds elsewhere in the Sydney and adjacent basins host similar palynofloras rich in leiospherid algae and acritarchs as evident from

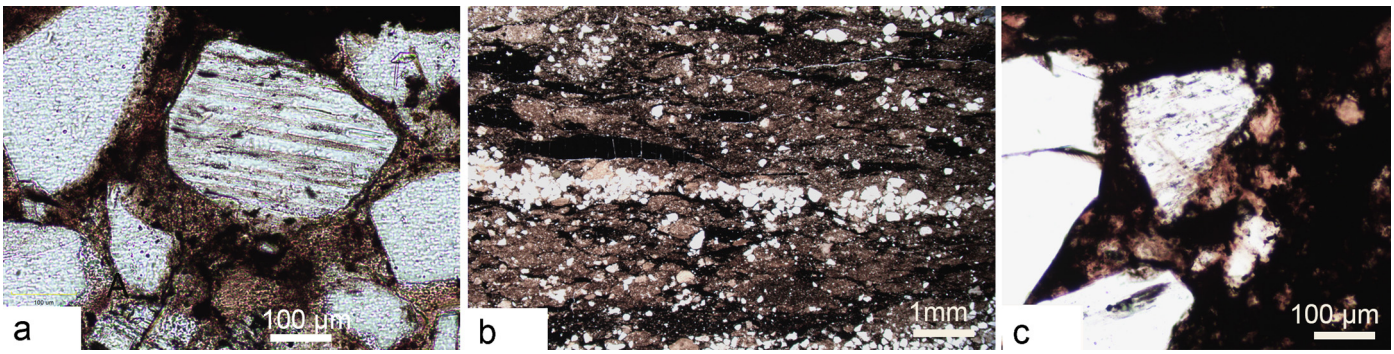

Fig. 8. Photomicrographs in non-polarized light of thin sections of sandstone/microbreccia from the 'dead zone' at Frazer Beach with organic-rich matrix filling pore spaces, possibly the result of bioclogging. **a)** Quartz and feldspar grains in an organic matrix; **b)** Quartz grains, clay clasts and coal fragments bound by organic matrix. **c)** Angular quartz and feldspar grains in organic matrix.

low-resolution sampling of successions in bore cores across the region (Helby, 1970; de Jersey, 1979; Fielding et al., 2019). Importantly, a recent study from the Galilee Basin, substantially more remote from coastal settings, revealed a similar lithological and palynological succession with anomalously high algal abundances—in that case interpreted to signify a possible marine incursion in response to foreland loading (Wheeler et al., in press). Epicratonic basins in the Australian continental interior (Cooper-Simpson basin complex) are also characterized by a sharp transition from coal-bearing sluggish fluvial to ephemeral lacustrine deposits (Radke, 2009) but the palynology of these successions has not been investigated in detail.

This early recovery phase is equivalent to the global algal/acritarch event outlined by Rampino and Eshet (2018) and possibly also equates to the acritarch blooms of freshwater aspect in marine EPE deposits described by van Soelen et al. (2018) from Greenland and van Soelen and Kürschner (2018) from Finnmark, Norway. Most of the algal cysts in the studied interval bear imprints of pyrite framboids (Fig. 6k–n)—a feature also documented from marine EPE successions (China; Shen et al., 2007; Australia; Bond and Wignall, 2010; Xie et al., 2017) and interpreted as signaling enhanced microbial activity and degradation of organic matter in anoxic and, in some cases also brackish, aqueous conditions (Grice et al., 2005; Kershaw et al., 2012). Estimated duration: 20,000–30,000 yrs.

4.4.4. Phase IV. Vegetation recovery—spore spike and the first vascular plants (>160 cm above the coal)

Notable quantities of vascular plants reappear at 160 cm above the level of the EPE, and a few centimeters above the uppermost possible tuff band, in beds that still contain significant numbers of algal cysts (Fig. 3). The palynological assemblages reveal a pulse in the abundance of fern and lycophyte spore taxa, most notably *Brevitriletes bulliensis*, *Playfordiaspora crenulata*, *Densoisporites playfordii*, *Apiculatisporites* spp., *Cyclogranulatisporites* sp., together with various, first appearances (for this succession) of non-taeniate gymnosperm pollen types (especially *Vitreisporites pallidus* and *Falcisporites australis*). Fossil leaves and stems of equisetaleans, isoetalean lycophytes, voltzialean conifers, probable ginkgoaleans, and peltaspermalean seed-ferns also appear at this level (Fig. 5). These spore-pollen and macrofossil assemblages characterize a pioneering open vegetation (Fig. 7) dominated by opportunistic (ruderal) herbaceous pteridophytes and small-leafed sclerophyllous gymnosperms.

Ruderal plants thrived in the aftermath of the EPE owing to their ability to grow and reproduce rapidly (both sexually and asexually) in disturbed conditions under a strongly seasonal climate (Grime, 2001). Their small disseminules also facilitated long-distance dispersal, typically enabling taxa to occupy broad geographic ranges. Despite the resurgence of vascular plants at this level in the studied succession, their diversity remained low and their leaves tend to be diminutive with thick cuticles attesting to continuing harsh environmental conditions. The short stratigraphic interval/lag time (160 cm: 15,000–30,000 yrs) between the EPE and the appearance of new vascular plant taxa shows that speciation in some surviving lineages occurred rapidly. This observation may also impact the interpretation of similar floras elsewhere that contain typical Triassic elements interpreted to be of pre-EPE age (Saxena et al., 2018; Blomenkemper et al., 2018). These might instead represent early post-extinction (though still Permian) recovery floras with a few holdover taxa.

Estimated duration: initiating 15,000–20,000 yrs after the EPE and persisting with increased diversity and variations in abundance of plant groups for several million years.

4.4.5. Phase V: Recovery of peat-forming ecosystems (>700 m above the coal)

Peat-forming ecosystems took a long time to re-establish in the Sydney Basin, and palynofloras of fully recovered terrestrial vegetation were not detected in this high-resolution study as they reappear ~700 m above the Vales Point coal (see Mays et al., in press). The youngest coaly strata globally, following the end-Permian event, are thin beds of carbonaceous shale to paper coal, dominated by the matted leaves of the seed-fern *Dicroidium*, identified in the Terrigal Formation (upper Spathian: ~248 Ma) of the Sydney Basin (Retallack et al., 1996). Coals approaching economic thicknesses appear only in the Anisian–Ladinian of southeastern Gondwana and western Europe some 10 Myrs after the EPE (Retallack et al., 1996).

4.5. Taxonomic versus ecological crisis?

Eruption of the Siberian Traps through a thick sequence of coal-bearing strata in the Tunguska Basin is generally inferred to be the underlying cause of the EPE. We do not dispute the remarkable scale or potential significance of that basaltic volcanism. However, we note that the convergent-margin volcanism that more-or-less encircled the amalgamated continents at the close of the Paleozoic (Geißle et al., 2008; Shen et al., 2013; Liao et al., 2016; Riel et al., 2018; Jessop et al., 2019) essentially formed a 'Pangean ring of fire' (Fig. 3c) that likely also impacted ecosystems around the fringe of the supercontinent. Elevated levels of activity along this volcanic belt in the late Permian, including along the eastern Australian margin (Rosenbaum, 2018; Jessop et al., 2019) may have strongly influenced environments and biotas of continental-margin basins and contributed to the intensity of the EPE in both terrestrial and shallow marine settings.

The sudden and Gondwanan-wide extinction of glossopterids and cordaitaleans in the continental record of the EPE has been

discussed mainly in terms of changes in taxonomic diversity, and some authors have claimed that the EPE, instead of signaling a decline in plant taxa, expresses no or little extinction (Schneebeli-Hermann et al., 2015, 2017; Nowak et al., 2019). By focusing exclusively on taxonomic diversity, one crucial aspect is overlooked, namely the ecological impact caused by the disappearance of forests. Although glossopterids overwhelmingly dominated the vegetation and the fossil macrofloral record in terms of abundance, they only represented a minor part of the overall end-Permian diversity. Individual Australian late Permian leaf assemblages, typically contain less than 10 *Glossopteris* species (Sydney Basin: Holmes, 1995; Bowen Basin: McLoughlin, 1994a, 1994b). It is evident that many of the taxonomically diverse, understorey spore-producing, vascular plant families (of ferns, horsetails and club-mosses) survived the EPE as noted in this study, but a mass-kill of vegetation and removal of key-groups occurred similar to that at the Cretaceous–Paleogene boundary event (Vajda and Bercovici, 2014). Secondly, erosion of older deposits following the collapse of the glossopterid forests, resulted in some typical Permian palynomorph taxa and dispersed cuticles being reworked into younger sediments in many sections, thus blurring the signal of extinction in thick, sparsely sampled sections from 'sharp' to 'attenuated' (Nowak et al., 2019). We can now address this issue with our high-resolution investigation of the palynological and macrofloral signals from a sedimentologically well-characterized succession that reveal a sudden disappearance of the broad-leafed glossopterid forests and their replacement by a vegetation dominated by sclerophyllous peltasperms and conifers together with various herbaceous pteridophytes.

The results show that although many plant groups disappeared from the local ecosystems for a restricted interval, they return to the post-event ecosystem reflected in the spore spike, where these taxa (at least at family level) survived in regional refugia, possibly at higher altitudes, or in coastal settings where conditions were consistently cooler and/or wetter. Although some of the survivors constituted the pioneer vegetation during the earliest post-extinction (possibly earliest Triassic) recovery interval, new species also emerged. We attribute the very rapid appearance in the macroflora of the studied section of the new, low-diversity, drought-tolerant plant associations (dominated by conifers and the seed fern *Lepidopteris*) to represent immigration probably from relatively warmer and better-drained regions, including upland settings, that locally hosted taxa pre-adapted to drought-tolerance. These drier-setting plants probably occurred in small populations and had low preservational potential in the late Permian. Similar ecological patterns have been described from the Karoo Basin, South Africa, with rapid radiations of new taxa after the main extinction phase that are partly attributed to waves of immigration of drought-adapted biota from other regions of Pangea (Sahney and Benton, 2008).

In contrast, glossopterids, which dominated the cool Permian wetland forest communities in terms of biomass, became extinct, resulting in enormous consequences for landscape coverage, ecosystem structure, food webs, and caused substantial perturbations to the hydrological and carbon cycles of the entire biosphere.

5. Conclusions

We conclude that the end-Permian destruction of the *Glossopteris*-dominated wetland forests in the cool high paleolatitudes of southern Gondwana was probably linked to a tipping point in atmospheric warmth and/or the availability of moisture associated with intensified seasonality at the close of the Permian. Similarities in the signature of the vegetation turnover between the end-Permian and end-Cretaceous events even ask the question whether short term lowering in light-levels may have influenced the EPE. At high resolution, the EPE in the studied successions is marked by a pronounced change from coal (floodbasin mire) to a carbonaceous mudstone (lacustrine deposition) similar to that described recently from the Galilee Basin in northern Australia. The extinction was followed by a short 'dead zone' characterized only by charcoal, wood fragments, and fungi that represents an interval of wildfire and saprotrophic breakdown of organic matter. Ponding of floodplains initiated during this 'fungal and wildfire event' and continued for an extended interval during which time laminated sediments lacking bioturbation were deposited. Maximum expression of the ponding is evidenced by an 'acritarch/algal event'. We interpret most of these cysts to represent green algae of freshwater conditions, although the variation in algal assemblages through the succession probably reflects temporal variation in factors such as nutrient status, temperature, salinity and/or pH. The surge in algal/acritarch abundance is similar to the peak in these remains reported from Northern Hemisphere marine records. Our study shows that the massive quantities of algae that flourished in these floodplain lakes must have been flushed into marine environments. We use our high-resolution succession as a template for interpreting the global fungal/algal/acritarch events and propose that the acritarch event reported in the marine EPE record elsewhere in fact incorporated abundant continentally derived algae (typified by acritarchs lacking or with reduced processes) combined with marine algal blooms resulting from eutrophication of nearshore marine environments.

Our discovery of an *in situ* macroflora of Triassic aspect in laminated sediments just 1.6 m above the uppermost Permian coal seam reveals the abruptness of the extinction and the local rapidity in recovery of selected plant groups. Our study also reveals that a few components of the palynoflora encountered in sandstones above this level are reworked, e.g. the Carboniferous pollen *Cannanoropolis*) and possibly the *Glossopteris*-complex (taeniate pollen). This feature may obscure the pattern of vegetation turnover in other studies (e.g. Nowak et al., 2019). Although plant recovery is evident both in the macro- and microfloras at 1.6 m above the EPE, plant productivity remained exceedingly low through the entire post-EPE succession at Frazer Beach. Productivity did not approach typical late Permian levels within the studied succession. Our results show that lowland deforestation at the EPE (loss of the *Glossopteris* forests) had enormous long-term effects on biodiversity, terrestrial community structure, climate and continental landscapes, and also greatly influenced marine ecosystems.

Acknowledgements

This research was funded by the Swedish Research Council (VR grant 2015-4264 to V.V., and VR grants 2014-5234 and 2018-04527 to S.M.); by the Royal Swedish Academy of Sciences, and by a collaborative research grant from the National Science Foundation (EAR-1636625 to C.R.F. and T.D.F.).

Appendix A. Supplementary material

Supplementary material related to this article can be found online at https://doi.org/10.1016/j.epsl.2019.115875.

References

Amiruddin, 2014. A review on Permian to Triassic active or convergent margin in southeasternmost Gondwanaland: possibility of exploration target for tin and hydrocarbon deposits in the eastern Indonesia. J. Geol. Indones. 4, 31–41.

Aragão, L.E.O., Malhi, Y., Barbier, N., Lima, A., Shimabukuro, Y., Anderson, L., Saatchi, S., 2008. Interactions between rainfall, deforestation and fires during recent years in the Brazilian Amazonia. Philos. Trans. R. Soc. Lond. B, Biol. Sci. 363, 1779–1785. https://doi.org/10.1098/rstb.2007.0026.

Baker, R.T., 1931. On a specimen of fossil timber from the Sydney Harbour colliery. J. Proc. R. Soc. N. S. W. 65, 96–111.

Batten, D.J., 1996. Palynofacies and palaeoenvironmental interpretation. In: Jansonius, J., McGregor, D.C. (Eds.), Palynology: Principles and Applications 3. American Association of Stratigraphic Palynologists Foundation, Los Angeles, pp. 1011–1064 (Chapter 26A).

Blakey, R., 2005. Global Earth history. http://jan.ucc.nau.edu/~rcb7/RCB.html. (Accessed 10 August 2019).

Blomenkemper, P., Kerp, H., Abu Hamad, A., DiMichele, W.A., Bomfleur, B., 2018. A hidden cradle of plant evolution in Permian tropical lowlands. Science 362, 1414–1416.

Bond, D.P.G., Wignall, P.B., 2010. Pyrite framboid study of marine Permian-Triassic boundary sections: a complex anoxic event and its relationship to contemporaneous mass extinction. Geol. Soc. Am. Bull. 122, 1265–1279.

Brookfield, M.E., Stebbins, A.G., Rampino, M., Hannigan, R.E., 2018. Significance of carbon, nitrogen and their isotopic changes in a Permian-Triassic non-marine boundary section at Carlton Heights (Karoo Basin), South Africa. J. Afr. Earth Sci. 8, 170–177.

Burenina, T.A., Onuchin, A.A., Fedotova, E.D., 2014. Hydrological effect of orest logging in Boreal zone of Siberia. In: Roberts, N.C. (Ed.), Forest Ecosystems—Biodiversity, Management and Conservation. Nova Science Publishers, New York, pp. 117–147.

Burgess, S.D., Bowring, S., Shen, S.-z., 2014. High-precision timeline for Earth's most severe extinction. Proc. Natl. Acad. Sci. USA 111, 3316–3321.

Burgess, S.D., Muirhead, J.D., Bowring, S.A., 2017. Initial pulse of Siberian Traps sills as the trigger of the end-Permian mass extinction. Nat. Commun. 8, 164. https://doi.org/10.1038/s41467-017-00083-9.

Clymo, R.S., 1987. Rainwater-fed peat as a precursor to coal. In: Scott, A.C. (Ed.), Coal and Coal-Bearing Strata: Recent Advances. In: Geol. Soc. Spec. Publ., vol. 32, pp. 17–23.

Costa, M.H., Pires, G.F., 2010. Effects of Amazon and central Brazil deforestation scenarios on the duration of the dry season in the arc of deforestation. Int. J. Climatol. 30, 1970–1979. https://doi.org/10.1002/joc.2048.

Cui, X.F., Graf, H.F., Langmann, B., Chen, W., Huang, R.H., 2007. Hydrological impacts of deforestation on the southeastern Tibetan Plateau: a model study. Earth Interact. 11, 1–18. https://doi.org/10.1175/EI223.1.

de Jersey, N.J., 1979. Palynology of the Permian-Triassic Transition in the Western Bowen Basin. Geol. Surv. Qd Publ. 374, Palaeontol. Pap. 46, pp. 1–61.

Díaz, M.F., Bigelow, S., Armesto, J.J., 2007. Alteration of the hydrologic cycle due to forest clearing and its consequences for rainforest succession. For. Ecol. Manag. 244, 32–40. https://doi.org/10.1016/j.foreco.2007.03.030.

Diessel, C.F.K., Smyth, M., 1995. Petrographic constituents of Australian coals. In: Ward, C.R., Harrington, H.J., Mallett, C.W., Beeston, J.W. (Eds.), Geology of Australian Coal Basins. In: Geological Society of Australia Incorporated, Coal Geology Group Special Publication, vol. 1, pp. 63–81.

Eshet, Y., Rampino, M.R., Visscher, H., 1995. Fungal event and palynological record of ecological crisis and recovery across the Permian–Triassic boundary. Geology 23, 967–970.

Fielding, C.R., Sliwa, R., Holcombe, R.J., Jones, A.T., 2001. A new palaeogeographic synthesis for the Bowen, Gunnedah and Sydney basins of eastern Australia. In: Hill, K.C., Bernecker, T. (Eds.), Eastern Australasian Basins Symposium 2001: A Refocused Energy Perspective for the Future. In: Petroleum Exploration Society of Australia Special Publication, vol. 1. Melbourne, pp. 269–278.

Fielding, C.R., Frank, T.D., McLoughlin, S., Vajda, V., Mays, C., Tevyaw, A.P., Winguth, A., Winguth, C., Nicoll, R.S., Bocking, M., Crowley, J.L., 2019. Age and pattern of the southern high-latitude continental end-Permian extinction constrained by multiproxy analysis. Nat. Commun. 10, 1–12. https://doi.org/10.1038/s41467-018-07934-z.

Foster, C.B., 1979. Permian plant microfossils of the Blair Athol Coal Measures, Baralaba coal measures, and basal Rewan Formation of Queensland. Publ. - Geol. Surv. Qld. 372, 1–244.

Frank, T.D., Shultis, A.I., Fielding, C.R., 2015. Acme and demise of the late Palaeozoic ice age: a view from the southeastern margin of Gondwana. Palaeogeogr. Palaeoclimatol. Palaeoecol. 418, 176–192. https://doi.org/10.1016/j.palaeo.2014.11.016.

Geißle, M., Breitkreuz, C., Kiersnowski, H., 2008. Late Paleozoic volcanism in the central part of the Southern Permian Basin (NE Germany, W Poland): facies distribution and volcano-topographic hiati. Int. J. Earth Sci. (Geol. Rundsch.) 97, 973–989.

Gentry, A.H., Lopez-Parodi, J., 1980. Deforestation and increased flooding of the upper Amazon. Science 210, 1354–1356.

Grice, K., Cao, C.Q., Love, G.D., Bottcher, M.E., Twitchett, R.J., Grosjean, E., Summons, R.E., Turgeon, S.C., Dunning, W., Jin, Y.G., 2005. Photic zone euxinia during the Permian-Triassic superanoxic event. Science 307, 706–709. https://doi.org/10.1126/science.1104323.

Grime, J.P., 2001. Plant Strategies, Vegetation Processes, and Ecosystem Properties. John Wiley and Sons, Chichester. 419 pp.

Gulbranson, E.L., Isbell, J.L., Taylor, E.L., Ryberg, P.E., Taylor, T.N., Flaig, P.P., 2012. Permian polar forests: deciduousness and environmental variation. Geobiology 10, 479–495.

Haas, M., Baumann, F., Castella, D., Haghipour, N., Reusch, A., Strasser, M., Eglinton, T.I., Dubois, N., 2019. Roman-driven cultural eutrophication of Lake Murten, Switzerland. Earth Planet. Sci. Lett. 505, 110–117.

Haig, D., Martin, S.K., Mory, A.J., McLoughlin, S., Backhouse, J., Berrell, R.W., Kear, B.P., Hall, R., Foster, C.B., Shi, G.R., Bevan, J.C., 2015. Early Triassic (early Olenekian) life in the interior of East Gondwana: mixed marine-terrestrial biota from the Kockatea Shale, Western Australia. Palaeogeogr. Palaeoclimatol. Palaeoecol. 471, 511–533.

Helby, R.J., 1970. A Biostratigraphy of the Late Permian and Triassic of the Sydney Basin. PhD Thesis. Sydney University, Sydney. 479 pp. (unpublished).

Hicks, J.F., Johnson, K.R., Obradovich, J.D., Tauxe, L., Clark, D., 2002. Magnetostratigraphy and geochronology of the Hell Creek and basal Fort Union Formations of southwestern North Dakota and a recalibration of the age of the Cretaceous-Tertiary boundary. In: Hartman, J.H., Johnson, K.R., Nichols, D.J. (Eds.), The Hell Creek Formation and the Cretaceous-Tertiary boundary in the Northern Great Plains: An Integrated Record of the End of the Cretaceous. In: GSA Spec. Pap., vol. 361, pp. 35–55.

Holmes, W.B.K., 1995. The Late Permian megafossil flora from Cooyal, New South Wales, Australia. In: Pant, D.D. (Ed.), Global Environment and Diversification of Plants through Geological Time. Birbal Sahni Centenary Volume. Birbal Sahni Institute of Palaeobotany, Lucknow, pp. 123–152.

Izart, A., Suarez-Ruiz, I., Bailey, J., 2015. Paleoclimate reconstruction from petrography and biomarker geochemistry from Permian humic coals in Sydney Coal Basin (Australia). Int. J. Coal Geol. 138, 145–157. https://doi.org/10.1016/j.coal.2014.12.009.

Jessop, K., Daczko, N.R., Piazolo, S., 2019. Tectonic cycles of the New England Orogen, eastern Australia: a review. Aust. J. Earth Sci. 66, 459–496. https://doi.org/10.1080/08120099.2018.1548378.

Kar, R., Ghosh, A.K., 2018. First record of Reduviasporonites from the Permian–Triassic transition (Gondwana Supergroup) of India. Alcheringa. https://doi.org/10.1080/03115518.2018.1465595. In press.

Kershaw, S., Crasquin, S., Li, Y., Collin, P.-Y., Forel, M.-B., Mu, X., Baud, A., Wang, Y., Xie, S., Maurer, F., Guo, L., 2012. Microbialites and global environmental change across the Permian–Triassic boundary: a synthesis. Geobiology 10, 25–47. https://doi.org/10.1111/j.1472-4669.2011.00302.x.

Laurie, J.R., Bodorkos, S., Nicoll, R.S., Crowley, J.L., Mantle, D.J., Mory, A.J., Wood, G.R., Backhouse, J., Holmes, E.K., Smith, T.E., Champion, D.C., 2016. Calibrating the middle and late Permian palynostratigraphy of Australia to the geologic time scale via U–Pb zircon CA-IDTIMS dating. Aust. J. Earth Sci. 63, 701–730. https://doi.org/10.1080/08120099.2016.1233456.

Liao, Z., Hu, W., Cao, J., Wang, X., Yao, S., Wua, H., Wan, Y., 2016. Heterogeneous volcanism across the Permian–Triassic Boundary in South China and implications for the Latest Permian Mass Extinction: new evidence from volcanic ash layers in the Lower Yangtze Region. J. Asian Earth Sci. 127, 197–210.

Lindgren, S., 1981. Remarks on the taxonomy, botanical affinities, and distribution of leiospheres. Stockh. Contrib. Geol. 38, 1–20.

Looy, C., Twitchett, R.J., Dilcher, D.L., van Konijnenburg-van Cittert, J.H.A., 2001. Life in the end-Permian dead zone. Proc. Natl. Acad. Sci. USA 98, 7879–7883.

Marengo, J.A., Espinoza, J.C., 2015. Extreme seasonal droughts and floods in Amazonia: causes, trends and impacts. Int. J. Climatol. 36, 1033–1050.

Mays, C., Vajda, V., Frank, T.D., Fielding, C.R., Tevyaw, A.P., McLoughlin, S., in press. Refined Permian–Triassic floristic timeline reveals early collapse and delayed recovery of south polar terrestrial ecosystems. GSA Bull. https://doi.org/10.1130/B35355.1.

McLoughlin, S., 1993. Plant fossil distributions in some Australian Permian non-marine sediments. Sediment. Geol. 85, 601–619.

McLoughlin, S., 1994a. Late Permian plant megafossils from the Bowen Basin, Queensland, Australia: Part 2. Palaeontogr. B 231, 1–29.

McLoughlin, S., 1994b. Late Permian plant megafossils from the Bowen Basin, Queensland, Australia: Part 3. Palaeontogr. B 231, 31–62.

McLoughlin, S., 2011. Glossopteris – insights into the architecture and relationships of an iconic Permian Gondwanan plant. J. Bot. Soc. Bengal 65, 93–106.

McLoughlin, S., Maksimenko, A., Mays, C., 2019. A new high-paleolatitude permineralized peat flora from the late Permian of the Sydney Basin, Australia. Int. J. Plant Sci. 180, 513–539. https://doi.org/10.1086/702939.

Metcalfe, I., Crowley, J.L., Nicoll, R.S., Schmitz, M., 2015. High-precision U-Pb CA-TIMS calibration of Middle Permian to Lower Triassic sequences, mass extinction and extreme climate-change in eastern Australian Gondwana. Gondwana Res. 28, 61–81. https://doi.org/10.1016/j.gr.2014.09.002.

Metcalfe, I., Nicoll, R.S., Willink, R.J., 2008. Conodonts from the Permian-Triassic transition in Australia and position of the Permian-Triassic boundary. Aust. J. Earth Sci. 55, 365–377.

Niklas, K.J., 1994. Predicting the height of fossil plant remains: an allometric approach to an old problem. Am. J. Bot. 81, 1235–1242.

Noorbergen, L.J., Abels, H.A., Hilgen, F.J., Robson, B.E., de Jong, E., Dekkers, M.J., Krijgsman, W., Smit, J., Collinson, M.E., Kuiper, K.F., 2018. Conceptual models for short-eccentricity-scale climate control on peat formation in a lower Palaeocene fluvial system, north-eastern Montana (USA). Sedimentology 65, 775–808.

Nowak, H., Schneebeli-Hermann, E., Kustatscher, E., 2019. No mass extinction for land plants at the Permian–Triassic transition. Nat. Commun. 10, 384. https://doi.org/10.1038/s41467-018-07945-w.

Payne, J.L., Clapham, M.E., 2012. End-Permian extinction in the oceans: an ancient analog for the Twenty-First Century. Annu. Rev. Earth Planet. Sci. 40, 89–111.

Radke, B., 2009. Hydrocarbon and Geothermal Prosepctivity of Sedimentary Basins in Central Australia; Warburton, Cooper, Perdirka, Galilee, Simpson and Eromanga Basins. Geoscience Australia Rec. 2009/25, pp. 1–161.

Rampino, M., Eshet, Y., 2018. The fungal and acritarch events as time markers for the latest Permian mass extinction: an update. Geosci. Front. 9, 147–154. https://doi.org/10.1016/j.gsf.2017.06.005.

Renne, P.R., Arenillas, I., Arz, J.A., Vajda, V., Gilabert, V., Bermúdez, H.D., 2018. Multiproxy record of the Chicxulub impact at the Cretaceous-Paleogene boundary from Gorgonilla Island, Colombia. Geology 46, 547–550.

Retallack, G.J., 1999. Postapocalyptic greenhouse paleoclimate revealed by earliest Triassic paleosols in the Sydney Basin, Australia. Bull. Geol. Soc. Am. 111, 52–70.

Retallack, G.J., 2005. Earliest Triassic claystone breccias and soil-erosion crisis. J. Sediment. Res. 75, 679–695.

Retallack, G.J., Veevers, J.J., Morante, R., 1996. Global coal gap between Permian–Triassic extinction and Middle Triassic recovery of peat-forming plants. Geol. Soc. Am. Bull. 108, 195–207. https://doi.org/10.1130/0016-7606(1996)108<0195:GCGBPT>2.3.CO;2.

Riel, N., Jaillarda, E., Martelat, J-E., Guillot, S., Braun, J., 2018. Permian-Triassic Tethyan realm reorganization: implications for the outward Pangea margin. J. South Am. Earth Sci. 81, 78–86.

Rosenbaum, G., 2018. The Tasmanides: Phanerozoic tectonic evolution of eastern Australia. Annu. Rev. Earth Planet. Sci. 46, 291–325.

Ruprecht, J.K., Schofield, N.J., 1991a. Effects of partial deforestation on hydrology and salinity in high salt storage landscapes. I. Extensive block clearing. J. Hydrol. 129, 19–38. https://doi.org/10.1016/0022-1694(91)90042-G.

Ruprecht, J.K., Schofield, N.J., 1991b. Effects of partial deforestation on hydrology and salinity in high salt storage landscapes. II. Strip, soils and parkland clearing. J. Hydrol. 129, 39–55. https://doi.org/10.1016/0022-1694(91)90043-H.

Sahney, S., Benton, M.J., 2008. Recovery from the most profound mass extinction of all time. Proc. R. Soc. B 275, 759–765.

Saxena, A., Singh, K.J., Cleal, C.J., Chandra, S., Goswami, S., Shabbar, H., 2018. Development of the Glossopteris flora and its end Permian demise in the Tatapani–Ramkola Coalfield, Son–Mahanadi Basin, India. Geol. J. 54, 2472–2494. https://doi.org/10.1002/gj.3307.

Schneebeli-Hermann, E., Kürschner, W.M., Kerp, H., Bomfleur, B., Hochuli, P.A., Bucher, H., Ware, D., Roohi, G., 2015. Vegetation history across the Permian–Triassic boundary in Pakistan (Amb section, Salt Range). Gondwana Res. 27, 911–924.

Schneebeli-Hermann, E., Hochuli, P.A., Bucher, H., 2017. Palynofloral associations before and after the Permian-Triassic mass extinction, Kap Stosch, East Greenland. Glob. Planet. Change 155, 178–195.

Schulte, P., 2010et al.. The Chicxulub asteroid impact and mass extinction at the Cretaceous-Paleogene boundary. Science 327, 1214–1218.

Shen, J., Algeo, T.J., Hu, Q., Xu, G.Z., Zhou, L., Feng, Q.L., 2013. Volcanism in South China during the Late Permian and its relationship to marine ecosystem and environmental changes. Glob. Planet. Change 105, 121–134.

Shen, W., Lin, Y., Xu, L., Li, J., Wu, Y., Sung, Y., 2007. Pyrite framboids in the Permian-Triassic boundary section at Meishan, China: evidence for dysoxic deposition. Palaeogeogr. Palaeoclimatol. Palaeoecol. 253, 323–331. https://doi.org/10.1016/j.palaeo.2007.06.005.

Shi, G.R., Waterhouse, J.B., McLoughlin, S., 2010. The Lopingian of Australasia: a review of biostratigraphy, correlations, palaeogeography and palaeobiogeography. Geol. J. 45, 230–263. https://doi.org/10.1002/gj.1213.

Slater, B.J., McLoughlin, S., Hilton, J., 2015. A high-latitude Gondwanan lagerstätte: the Permian permineralised peat biota of the Prince Charles Mountains, Antarctica. Gondwana Res. 27, 1446–1473. https://doi.org/10.1016/j.gr.2014.01.004.

Spalletti, L.A., Limarino, C.O., 2017. The Choiyoi magmatism in south western Gondwana: implications for the end-permian mass extinction—a review. Andean Geol. 44, 328–338. https://doi.org/10.5027/andgeoV44n3-a05.

Stan, F., Neculau, G., Zaharia, L., Ioana-Toroimac, G., 2014. Evapotranspiration variability of different plant types at Romanian experimental evapometric measurement stations. Climatologie 11, 85–90.

Stanley, S.M., 2016. Estimates of the magnitudes of major marine mass extinctions in earth history. Proc. Natl. Acad. Sci. USA 113, E6325–E6334. https://doi.org/10.1073/pnas.1613094113.

Tewari, R., Ram-Awatar, Pandita, S.K., McLoughlin, S., Agnihotri, D., Pillai, S.S.K., Singh, V., Kumar, K., Bhat, G.D., 2015. The Permian-Triassic palynological transition in the Guryul Ravine section, Kashmir, India: implications for Tethyan – Gondwanan correlations. Earth-Sci. Rev. 14, 53–66.

Thomas, B.M., Willink, R.J., Grice, K., Twitchett, R.J., Purcell, R.R., Archbold, N.W., George, A.D., Tye, S., Alexander, R., Foster, C.B., Barber, C.J., 2004. Unique marine Permian-Triassic boundary section from Western Australia. Aust. J. Earth Sci. 51, 423–430. https://doi.org/10.1111/j.1400-0952.2004.01066.x.

Torres, I.C., Inglett, P.W., Brenner, M., Kenney, W.F., Reddy, K.R., 2012. Stable isotope (δ^{13}C and δ^{15}N) values of sediment organic matter in subtropical lakes of different trophic status. J. Paleolimnol. 47, 693–706.

Vajda, V., Bercovici, A., 2014. The global vegetation pattern across the Cretaceous-Paleogene mass-extinction interval – an integrated global perspective. Glob. Planet. Change 122, 29–49.

Vajda, V., McLoughlin, S., 2007. Extinction and recovery patterns of the vegetation across the Cretaceous–Palaeogene boundary — a tool for unravelling the causes of the end-Permian mass-extinction. Rev. Palaeobot. Palynol. 144, 99–112.

Van de Wetering, N., Esterle, J., Baublys, K., 2013a. Decoupling δ^{13}C response to palaeoflora cycles and climatic variation in coal: a case study from the Late Permian Bowen Basin, Queensland, Australia. Palaeogeogr. Palaeoclimatol. Palaeoecol. 386, 165–179.

Van de Wetering, N., Mendonça Filho, J.G., Esterle, J., 2013b. Palynofacies changes and their reflection on preservation of peat accumulation stages in the Late Permian coal measures of the Bowen Basin, Australia: a new system for coal palynofacies characterisation. Int. J. Coal Geol. 120, 57–70.

van Soelen, E.E., Kürschner, W.M., 2018. Late Permian to Early Triassic changes in acritarch assemblages and morphology in the Boreal Arctic: new data from the Finnmark Platform. Palaeogeogr. Palaeoclimatol. Palaeoecol. 505, 120–127. https://doi.org/10.1016/j.palaeo.2018.05.034.

van Soelen, E.E., Twitchett, R.J., Kürschner, W.M., 2018. Salinity changes and anoxia resulting from enhanced run-off during the late Permian global warming and mass extinction event. Clim. Past 14, 441–453. https://doi.org/10.5194/cp-14-441-2018.

Wang, X., Cawood, P.A., Zhao, H., Zhao, L., Grasby, S.E., Chen, Z-Q., Zhang, L., 2019. Global mercury cycle during the end-Permian mass extinction and subsequent Early Triassic recovery. Earth Planet. Sci. Lett. 513, 144–155.

Wells, J.A., Wilson, K.A., Abram, N.K., Nunn, M., Gaveau, D.L.A., Runting, R.K., Tarniati, N., Mengersen, K.L., Meijaard, E., 2016. Rising floodwaters: mapping impacts and perceptions of flooding in Indonesian Borneo. Environ. Res. Lett. 11, 064016. https://doi.org/10.1088/1748-9326/11/6/064016.

Wheeler, A., Van de Wetering, N., Esterle, J.S., Götz, A.E., in press. Palaeoenvironmental changes recorded in the palynology and palynofacies of a Late Permian Marker Mudstone (Galilee Basin, Australia). Palaeoworld. https://doi.org/10.1016/j.palwor.2018.10.005.

Woodward, C., Shulmeister, J., Larsen, J., Jacobsen, G.E., Zawadzki, A., 2014. The hydrological legacy of deforestation on global wetlands. Science 346, 844–847.

Xie, S., Algeo, T.J., Zhou, W., Ruan, X., Luo, G., Huang, J., Yan, J., 2017. Contrasting microbial community changes during mass extinctions at the Middle/Late Permian and Permian/Triassic boundaries. Earth Planet. Sci. Lett. 460, 180–191.

Ye, H., Shuan-Hong Zhang, S.-H., Yue Zhao, Y., 2014. Origin of two contrasting latest Permian–Triassic volcanic rock suites in the northern North China Craton: implications for early Mesozoic lithosphere thinning. Int. Geol. Rev. 56, 1630–1657. https://doi.org/10.1080/00206814.2014.951979.

Yin, H., Zhang, K., Tong, J., Yang, Z., Wu, S., 2001. The Global Stratotype Section and Point (GSSP) of the Permian-Triassic boundary. Episodes 24, 102–114.

Zhang, H.-R., Yang, T.-N., Zeng-Qian Hou, Z.-Q., Song, Y.-C., Ding, Y., Cheng, X.-F., 2013. Petrogenesis and tectonics of late Permian felsic volcanic rocks, eastern Qiangtang block, north-central Tibet: Sr and Nd isotopic evidence. Int. Geol. Rev. 55, 1017–1028. https://doi.org/10.1080/00206814.2012.759669.